

# Preparation of Sn-Ni alloy/Fluorographene Composite Coatings on Copper and Their Corrosion Behavior in NaCl Solution

Chuanyun Wan\*, Mengxin Ren, Xiya Liu

School of Chemical and Environmental Engineering, Shanghai Institute of Technology, Shanghai 201418, China

\*E-mail: [cywan@sit.edu.cn](mailto:cywan@sit.edu.cn)

Received: 24 June 2022 / Accepted: 4 November 2022 / Published: 30 November 2022

---

Fluorographene (FG) is studied to produce Sn-Ni/FG composite coatings to improve the corrosion resistance to an aggressive environment. Before use, fluorographene is functionalized with amino/oxygen-containing groups, making functionated fluorographene (FFG) dispersible in an aqueous solution. Sn-Ni/FG composite coatings are electrodeposited on a copper substrate by dispersing FFG into the electrolyte bath. The effect of FG on the microstructure and corrosion behavior of Sn-Ni coatings was analyzed by scanning electron microscopy (SEM) with energy-dispersive X-ray spectroscopy, X-ray diffraction (XRD), dynamic potential scanning, and electrochemical impedance spectroscopy (EIS). The amount of FG in the composite coatings was varied by changing the concentration of FG in the electrolyte bath. Sn-Ni/FG composite coatings with uniformly dispersed FG are successfully electrodeposited on copper substrates by dispersing functionalized fluorographene in a plating bath. Morphology examination of the coatings reveals that the addition of FG changes the grains from semispherical to interlock ridge. The crystallite size decreases and the compactivity of the composite increases with the increase in the FG content of the coatings when the content of FG in the bath is below 300 mg L<sup>-1</sup>. Compared to the pure Sn-Ni alloy coating, the corrosion resistance rate increases with the amount of FG in the coatings. However, too much FG in the plating bath will lead to an increase in the corrosion rate because of its limited dispersion stability. The small grain size, compact layer, and hindrance of FG to ion diffusion are responsible for the good corrosion resistance of the Sn-Ni/FG composite coating to an aggressive environment.

---

**Keywords:** Fluorographene; Sn-Ni/fluorographene composite; Corrosion resistance

## 1. INTRODUCTION

Sn-Ni alloys have wide technological applications due to their excellent wear, hardness and corrosion resistance properties [1-3]. The high hardness and high resistance of Sn-Ni alloys to tarnish make them potential alternatives to chromium or nickel coatings for decorative or protective applications

[4, 5]. Compared to pure Ni coatings or Sn coatings, the corrosion resistance of Sn-Ni alloy coatings is greatly improved both in neutral atmospheric environments and in acidic atmospheric environments [1, 6-10]. The composition of Sn-Ni alloys and the method of Sn-Ni codeposition are two factors that greatly affect their corrosion resistance [7,10,11]. For example, Sn-Ni alloys containing 33-35% nickel normally exhibit good corrosion resistance [10,12], and multilayer Sn-Ni alloys coated by pulsed sonoelectrolysis can obtain enhanced corrosion protection [11].

As an outer layer, the metallic layer must show good corrosion resistance for practical application. Applying metal matrix nanocomposite coatings containing non-metallic reinforcing phases such as  $\text{Al}_2\text{O}_3$  [13],  $\text{TiO}_2$  [14], SiC [15], diamond [16,17], carbon nanotubes [18], etc., is a good way to improve the anticorrosion properties of metallic layers. Among the non-metallic reinforcing phases, graphene has drawn much attention for its superior mechanical properties, electrical conductivity, chemical stability, and availability for surface functionalization [19-21] and has been used to obtain graphene-reinforced composite coatings for enhanced anticorrosion [22-25].

Graphene, as a single 2D carbon sheet, has difficulty producing uniform metal-graphene composites by conventional electrodeposition techniques due to its poor dispersibility in aqueous solutions [26]. Hence, water-soluble graphene oxide or reduced graphene oxide are often applied to prepare metal-graphene composite coatings to improve the corrosion resistance [22-24] or wear resistance [27] of metal coatings. Fluorographene (FG) is a graphene derivative that exhibits a high Young's modulus, high-quality insulator, and high thermal stability [28, 29]. Hence, FG has also attracted much attention for a variety of applications, such as nanocomposites [30], batteries [31] and lubricants [28, 32, 33]. Similar to graphene, the compatibility between FG and the environment is very important for its practical application. The surface functionalization of FG is an important strategy to broaden its application in water-based technology or oil systems [34, 35], and we have successfully prepared FG sheets functionalized with amino/oxygen-containing groups (FFG) by one-step exfoliation and functionalized fluoride graphite under ball milling conditions [36]. The obtained FFG has good dispersibility in an aqueous solution and is suitable for liquid-based technology.

According to the available literature and our knowledge, there are few reports on the preparation of Sn-Ni/FG and the investigation of the effect of FG on the physical and corrosion properties of Sn-Ni alloys. In this paper, we attempted to deposit FFG into a Sn-Ni alloy matrix to prepare a Sn-Ni/FG composite coated by the electrodeposition method. The morphology, microstructure, and electrochemical behavior of electrodeposited Sn-Ni/FG composite coatings containing different amounts of fluorinated graphene were determined and compared. The effect of FG content on the performance of Sn-Ni alloys for anticorrosion applications was studied in a neutral atmospheric environment.

## 2. EXPERIMENTAL

Fluorographene (FG) was obtained by the method provided in the literature [36]. Before use, FG was dispersed in a 50/50 alcohol aqueous solution under ultrasonic conditions (250 W, KQ-2000, Kunshan Co., Ltd.) for 20 min. After remaining stationary for 30 min, the upper dispersed solution was used for the addition of FG to the electroplating bath. The zeta potential of FG nanoparticles (FGs) in

water solution was detected by a nanoparticle size potentiometer (ZNS3600/Nano-ZS, Marlven). The Sn-Ni alloys were electrodeposited on copper cathodes in a pyrophosphate bath. The composition of the bath and the operating conditions are given in Table 1. Different concentrations of FG (50-500 mg L<sup>-1</sup>) were ultrasonically dispersed in electrolytes. The bath temperature was kept at 40 °C. The electrochemical codeposition of the Sn-Ni/FG composite coating in electrolytes with different FG contents was conducted at a cathodic current density of 1 A dm<sup>-2</sup> for 10 min. Sn-Ni/FG1 (2,3,4) is denoted as the Sn-Ni/FG composite obtained from the plating solution containing 0.05 (0.15, 0.3, 0.5) g L<sup>-1</sup> FG.

To investigate the effect of fluorographene on the deposition of metal ion discharge, the cathodic deposition process of Sn-Ni alloy was investigated by a cathodic linear polarization curve produced using a three-electrode system with a Cu disk (0.5 cm<sup>2</sup>) as the working electrode, Pt sheet (1 cm<sup>2</sup>) as the counter electrode, and calomel electrode as a reference electrode.

**Table 1.** Plating bath composition for Sn-Ni and Sn/Ni-FG composite coatings

Sample name	Bath composition	Concentration (g L <sup>-1</sup> )
Sn-Ni	K <sub>4</sub> P <sub>2</sub> O <sub>7</sub> · 3H <sub>2</sub> O	230
	NiSO <sub>4</sub> ·6H <sub>2</sub> O	45
	SnCl <sub>2</sub> ·2H <sub>2</sub> O	30
	NH <sub>4</sub> Cl	8
	Saccharin sodium	1
Sn-Ni/FG1 (2, 3, 4)	Sn-Ni bath +FFG	0.05 (0.15, 0.3, 0.5)

The morphology and composition of the Sn-Ni alloys were determined by scanning electron microscopy with energy dispersive *X-ray* spectroscopy (SEM, S-3400N, Hitachi, Japan) and transmission electron microscopy (TEM, Hitachi 600, Japan). The crystal structures of all samples were characterized by X-ray diffraction (XRD, RIGAKUD/MAX-cB, CuK α). X-ray photoelectron spectroscopy (XPS-Escalab 210) analysis of the composition of the Sn-Ni alloy was performed. The corrosion resistance behaviors of the Sn-Ni/FG composite coatings were analyzed in 5 wt. % NaCl using linear sweep voltammetry and electrochemical impedance spectroscopy (EIS) in a three-electrode cell in which Sn-Ni/FG composite coatings (0.5 cm<sup>2</sup>) were used as the working electrodes. Electrochemical impedance spectroscopy (EIS) experiments were performed from 0.1 Hz to 10<sup>5</sup> Hz at an amplitude of 10 mV. The scan rate of potentiodynamic polarization for the corrosion measurement was 1 mV s<sup>-1</sup>. All electrochemical tests were carried out on an electrochemical working station (Gamry Reference 600+).

### 3. RESULTS AND DISCUSSION

#### 3.1 Characterization of Fluorographene

Fig. 1a shows TEM images of FG. It is clear that FGs are ca. 20 nm nanosized flakes. The particle sizes are small enough to assume that the FGs are well embedded in the Sn-Ni matrix when they are used as external particles. XPS survey scan spectra of FG are shown in Fig. 1b. Except for the two major binding energy peaks at approximately 285 and 688 eV corresponding to carbon (1s) and fluoride (1s), there are two binding energies at approximately 400 and 532 eV corresponding to nitrogen (1s) and oxygen (1s), respectively.

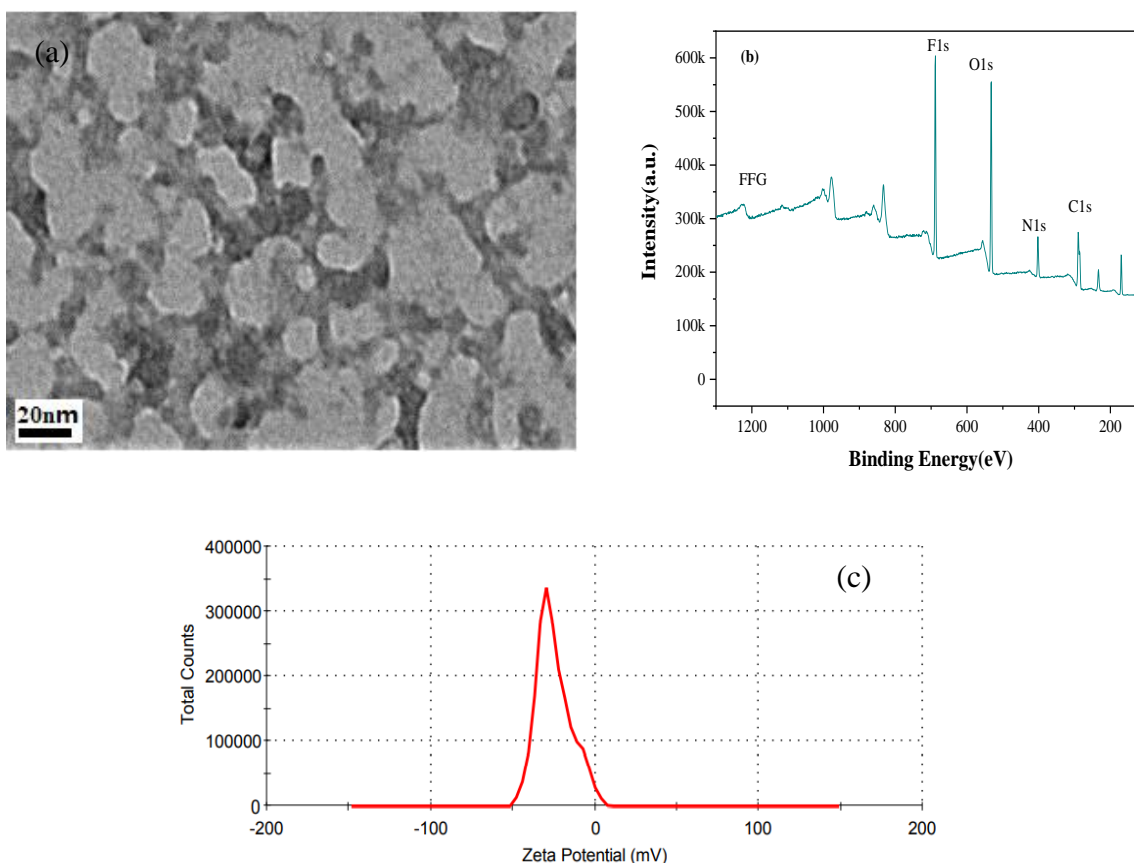


**Figure 1.** TEM image (a), XPS survey scan spectra (b) and zeta potential (c) of FFGs in aqueous solution.

The appearance of N and O indicates that the surface of the FG flakes contains amino/oxygen-containing groups, which allow FG flakes to be dispersed in an aqueous solution and suitable for metal-FG composite preparation [36]. The zeta potential of FGs in water solution is -24.8 mV, indicating a reasonable dispersibility and stability of FGs in an electroplating bath (Fig. 1c).

### 3.2 Electrodeposition of Sn-Ni/FG composite coating

To study the effect of FGs on the deposition of Sn-Ni, cathodic polarization curves were recorded and are presented in Fig. 2. Even though no obvious shift in the reduction potential is observed when FGs are added to the Sn-Ni electroplating solution, some interesting phenomena can be observed from the cathodic polarization curves.

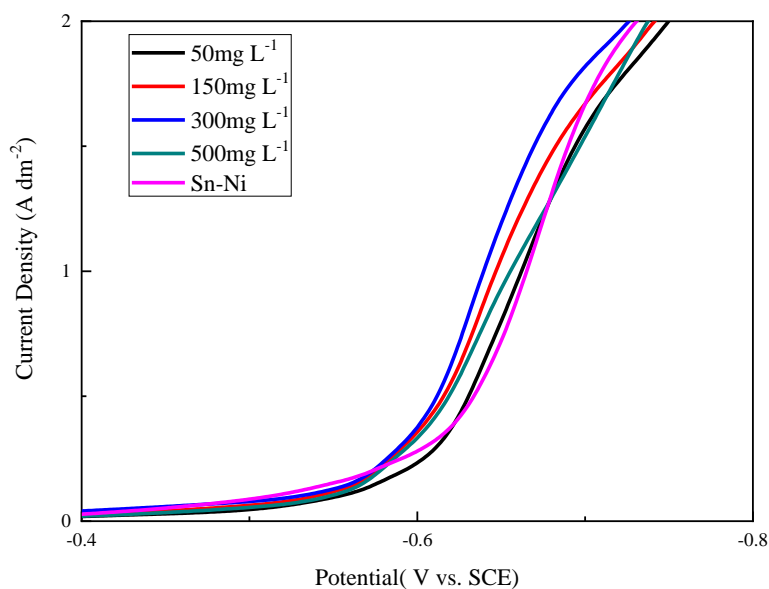


**Figure 2.** Cathodic polarization curves for the deposition of Sn-Ni and Sn-Ni/FG coatings produced from different plating baths.

The current density decreased at the lower reduction potential and increased when the reduction potential was sufficiently high in the FG-containing plating bath. This result indicates that the nanosized FGs affect the process more or less by adsorbing on the active sites of the cathodic surface. The adsorbed FFGs hinder crystal growth and favor the formation of a new nucleation site or reduction site, which leads to a fine grain size or changes the morphology of the composite at a lower potential polarization. When the polarization is sufficient, the increase in the active surface area of the cathode, owing to the conductivity of the adsorbed nanosized FFGS on the cathode, may lead to an increase in the current densities. This result is different from the fact that nonconductive MoS<sub>2</sub> particles decreased the reduction current density because of the decrease in the active surface area of the cathode owing to the adsorption of the MoS<sub>2</sub> nanoparticles [37].

### 3.3 Deposit characterization

X-ray diffractograms of the Sn-Ni and Sn-Ni/FG coatings are shown in Fig. 3. There are three main peaks at 43.4°, 50.6° and 74.2°, corresponding to the (110), (004) and (220) crystal faces, respectively, which are assigned to the Ni-rich Ni<sub>3</sub>Sn phase [9,38]. In comparison with the pure Sn-Ni

alloy, the intensity of Ni (110) peaks for Sn-Ni/FG composites are similar, but the (004) and (220) peaks present a gradual weakening trend with increasing FG content, indicating that FGs affect the electrodeposition process more or less when FGs exist in the plating bath. Even though the addition of FG does not obviously change the crystal orientation, the performance of Sn-Ni/FG will change due to the existence of FG. In addition, the characteristic diffraction peaks of FG were not observed in Fig. 3, indicating that the amount of FG was low or embedded in the Sn-Ni matrix, which resulted in no detection.

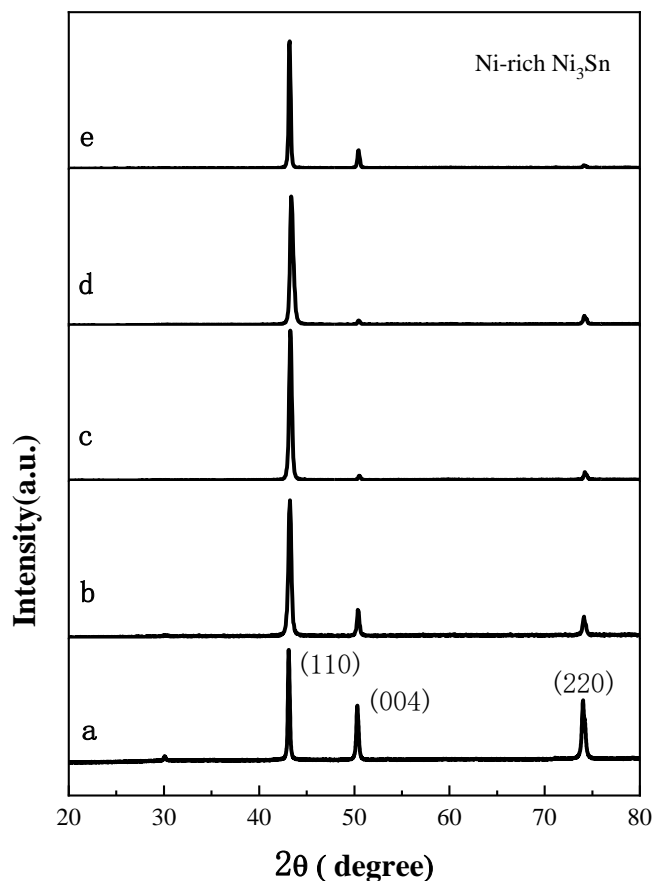


**Figure 3.** XRD patterns of Sn-Ni (a) and Sn-Ni/FG composite coatings (b, Sn-Ni/FG1; c, Sn-Ni/FG2; d, Sn-Ni/FG3; e, Sn-Ni/FG4).

According to the Byrd Scherrer formula [39], the average crystallite size for the Ni-rich phase in pure Sn-Ni and Sn-Ni/FG composite coatings can be calculated from the full width half maximum (FWHM) of the strong XRD peak. Therefore, the average crystallite size of the Ni-rich phase decreases from 27.0 nm ( $0.0 \text{ g L}^{-1}$ ) to 25.4 nm ( $0.05 \text{ g L}^{-1}$ ), 22.7 nm ( $0.15 \text{ g L}^{-1}$ ), 21.2 nm ( $0.3 \text{ g L}^{-1}$ ) and 25.7 nm ( $0.5 \text{ g L}^{-1}$ ). Compared to that of pure Sn-Ni alloys, the crystallite size decreases when the number of FGs is in a reasonable addition range and increases again when the amount of FGs is large enough. This may be explained by the fact that in the composite electrodeposition, the nanosized FG sheets enhance

nucleation by creating a disorder in the matrix, and the simultaneous diffusion of FG toward growing centers also helps retard crystal growth. The increase in nucleation growth and the retardation of crystal growth both lead to a decrease in grain size [24]. However, when the concentration of FG in the bath exceeded  $300 \text{ mg L}^{-1}$ , the grain refinement weakened. This phenomenon may be explained by the aggregation of FGs; the amount of FGs dispersed in the plating bath is too large and tends to agglomerate due to its metastability, resulting in a reduction in FGs diffusion and dispersibility [36].

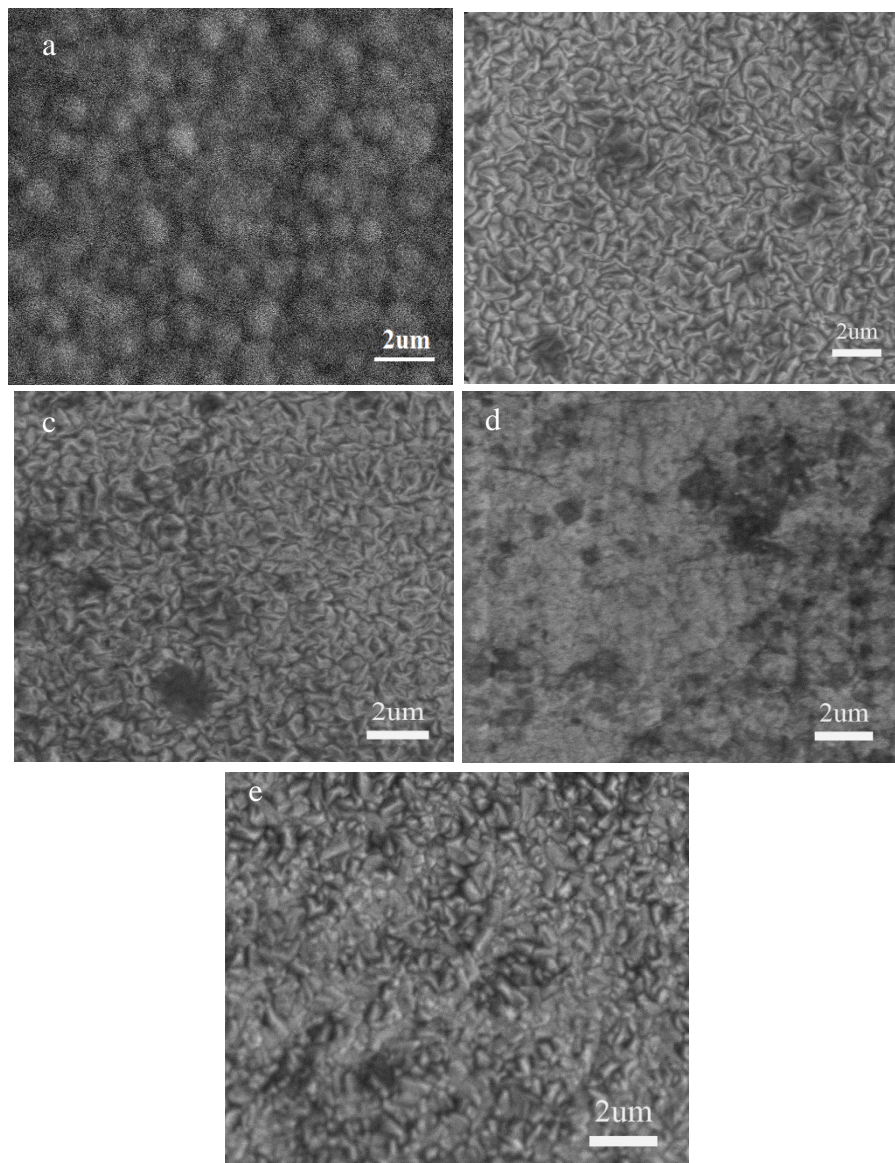


**Figure 4.** SEM images of (a) Sn-Ni, (b) Sn-Ni/FG1, (c) Sn-Ni/FG2, (d) Sn-Ni/FG3 and (e) Sn-Ni/FG4.

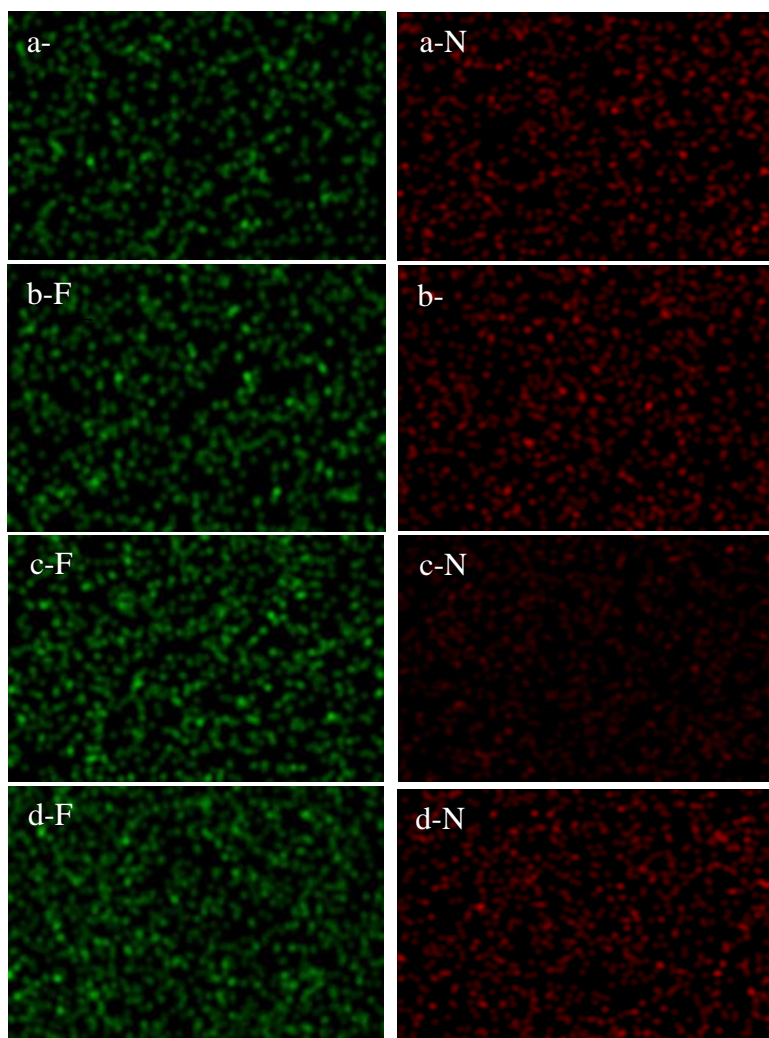


**Figure 5.** EDS mapping of F and N of samples (a) Sn-Ni/FG1, (b) Sn-Ni/FG2, (c) Sn-Ni/FG3, and (d) Sn-Ni/FG4.

The SEM images of Sn-Ni and FG-doped Sn-Ni/FG coatings (Sn-Ni/FG1, Sn-Ni/FG2, Sn-Ni/FG3, and Sn-Ni/FG4) are shown in Fig. 4. Obviously, the surface of the Sn-Ni alloy without FG is composed of semispherical grains. When fluorographene is added to the plating bath, the morphology of the alloy coating is changed from semispherical to an interlock ridge shape, of which the unit size is much smaller than that of spherical grains. With the increase in the concentration of fluorographene in the plating, the refinement of grains can be observed in the SEM images. The Sn-Ni/FG3 obtained from the plating bath containing  $300 \text{ mg L}^{-1}$  FG exhibits no evident grain boundary, indicating that its grain is highly refined. O and C may emerge from the adsorption of oxygen and carbon in the air atmosphere and the possible reaction of Sn-Ni alloy with them in air. F and N from the ammonia group on the FFG surface can be detected to indicate the codeposition of FFG with the Sn-Ni alloy. Fig. 5 shows the N and F mapping of the Sn-Ni/FG coating surfaces that support the uniformly dispersed incorporation of FG in the Sn-Ni alloy matrix. The F contents of the samples detected by EDS for Sn-Ni/FG1, Sn-Ni/FG2, Sn-Ni/FG3, and Sn-Ni/FG4 are 1.9, 3.2, 4.5, and 14.5 at. %, respectively, indicating that the amount of

FG incorporated in the Sn-Ni alloy increases with increasing amount of FFGS in the plating bath. All the results indicate that the codeposition of FFGS in the Sn-Ni alloy matrix successfully produced a Sn-Ni/FG composite coating.

### 3.4 Corrosion resistance of Sn-Ni/FG composites

Analysis of the electrochemical corrosion behaviors for the Sn-Ni and Sn-Ni/FG composite coatings were carried out in 5% NaCl solution at room temperature. Fig. 6 presents the potentiodynamic polarization curves of the Sn-Ni and Sn-Ni/FG composite coatings in 5% NaCl solution by polarizing the working electrode at a scan rate of  $1 \text{ mV s}^{-1}$ .

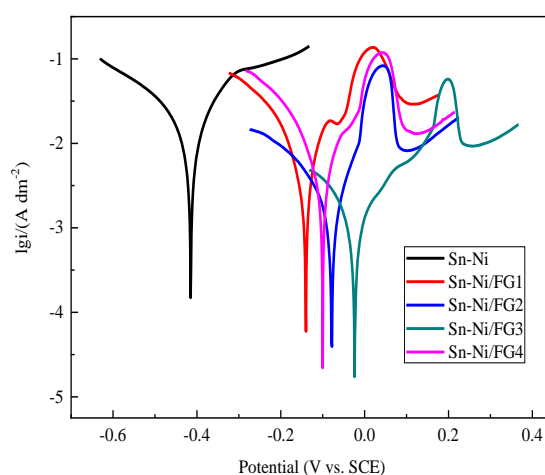


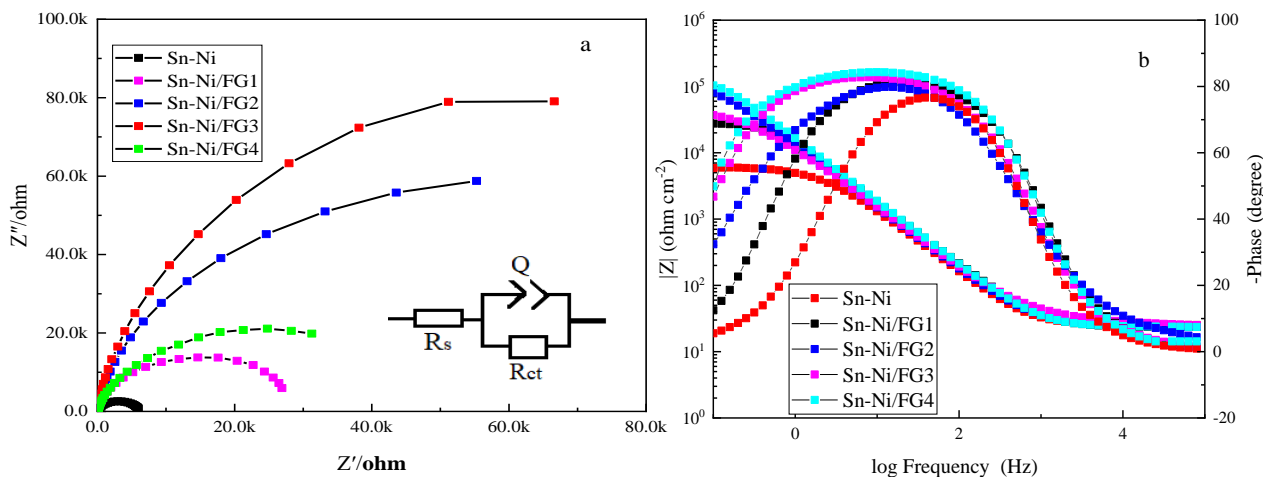
**Figure 6.** Potentiodynamic polarization curves of the Sn-Ni and Sn-Ni/FG composite coatings in 5% NaCl solution.

**Table 2.** Corrosion parameters determined from the Tafel plots for Sn-Ni and Sn-Ni/FG composite coatings

Sample	Sn-Ni	Sn-Ni/FG1	Sn-Ni/FG2	Sn-Ni/FG3	Sn-Ni/FG4
$I_{\text{corr}}$ ( $\text{mA dm}^{-2}$ )	7.550	3.687	0.950	0.634	3.623
$E_{\text{corr}}$ (V)	-0.415	-0.140	-0.080	0.024	-0.100

The  $E_{\text{corr}}$  and  $I_{\text{corr}}$  values were calculated using the Tafel extrapolation method and are given in Table 2. With the increase in the amount of FG to  $300 \text{ mg L}^{-1}$  in the bath, the corrosion potential of the Sn-Ni/FG coating shifts positively. Compared with that of the pure Sn-Ni alloy.  $I_{\text{corr}}$  also decreases with increasing FG content when the FG content is below  $300 \text{ mg L}^{-1}$ . With a further increase in the content

of FG in the bath, the corrosion potential of Sn-Ni/FG decreases, and  $I_{\text{corr}}$  increases when the FG concentration in the bath reaches  $500 \text{ mg L}^{-1}$ . These changes in the electrochemical parameters clearly show that the corrosion resistance of the Sn-Ni/FG composite coating is better than that of the pure Sn-Ni alloy and is related to its composition and surface morphology [2,23]. The best result of electrochemical corrosion for Sn-Ni/FG3 may be the result of its finest grain size observed in Fig. 4.

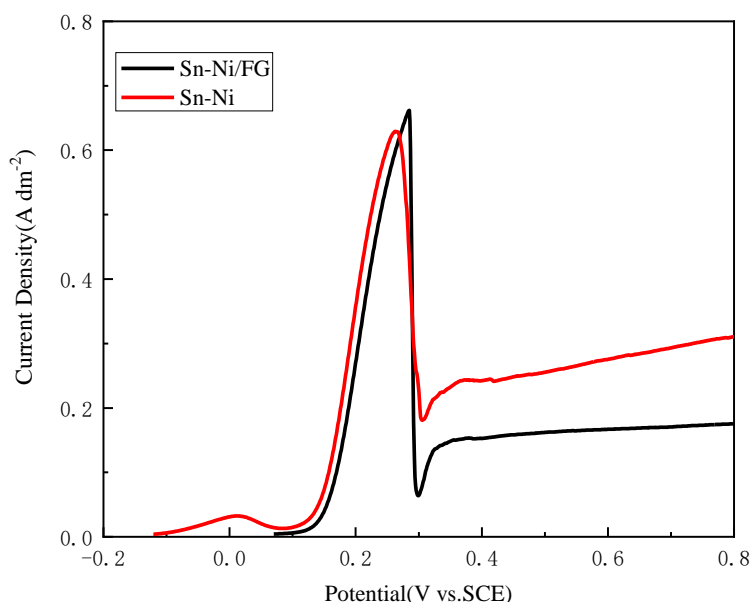


**Figure 7.** Electrochemical impedance spectra (EIS) for Sn-Ni, Sn-Ni/FG1, Sn-Ni/FG2, Sn-Ni/FG3 and Sn-Ni/FG4 composite coatings in 5% NaCl media: (a) Nyquist plots, (b) Bode plots.

The electrochemical impedance spectra (EIS) of the Sn-Ni and Sn-Ni/FG composite coatings were measured to determine the surface resistance in a 5% NaCl solution. EIS measurements were carried out at the respective OCP of the corresponding working electrode in the frequency range of 0.1 Hz to  $10^5$  Hz with an AC signal of 10 mV. The measured Nyquist plots for Sn-Ni, Sn-Ni/FG1, Sn-Ni/FG2, Sn-Ni/FG3, and Sn-Ni/FG4 composite coatings along with their Bode plots ( $|Z|$  vs.  $\log(\text{frequency})$ ) and phase vs.  $\log(\text{frequency})$ ) are shown in Fig. 7 a and Fig. 7 b, respectively. An electrical equivalent circuit (EEC) model is inserted in Fig. 7a to illustrate the interface reaction. In the given EEC model,  $R_s$  is the solution/electrolyte resistance between the reference electrode and the surface of the working electrode.  $R_{ct}$  and  $Q$  are the resistance to the charge transfer and double layer of constant phase element (CPE) parameter at the interface of the working electrode and solution, which replaces capacitance to characterize the homogeneity of the surface layer [23, 24]. The well-defined capacitive loop for Sn-Ni alloys indicates that the polarization resistance ( $R_p$ ) value, corresponding to the extent of the anti-corrosive character of the coatings [23], is similar to the charge transfer resistance ( $R_{ct}$ ). Table 3 summarizes the equivalent circuit parameters obtained by fitting the impedance data with Zview software using the proposed EEC model. The parameter  $n$  listed in Table 3 represents the extent of frequency dispersion in the capacitive component of double layer charging, which can characterize the inhomogeneous surface layer ( $n = 1$  for no dispersion) [23].

**Table 3.** Corrosion parameters obtained from impedance measurements by Nyquist plots

electrode	$R_{ct}/\Omega \text{ cm}^2$	n	$Q_{dl}/\mu\text{F cm}^{-2}$
Sn-Ni	$5980\pm35$	$0.92\pm0.03$	$16.57\pm0.52$
Sn-Ni/FG1	$30027\pm300$	$0.93\pm0.01$	$13.91\pm0.21$
Sn-Ni/FG2	$133630\pm346$	$0.94\pm0.03$	$11.51\pm0.04$
Sn-Ni/FG3	$201700\pm655$	$0.93\pm0.02$	$10.58\pm0.06$
Sn-Ni/FG4	$50480\pm550$	$0.87\pm0.04$	$17.70\pm0.18$

**Figure 8.** Anodic polarization curves of the Sn-Ni deposits and Sn-Ni/FG3 composite coating on a copper electrode in 5% NaCl solution at  $1 \text{ mV s}^{-1}$ 

For the Sn-Ni, Sn-Ni/FG1, Sn-Ni/FG2, and Sn-Ni/FG3 composite coatings, the polarization resistance ( $R_p$ ) was found to be  $5980 \Omega \text{ cm}^2$ ,  $30027 \Omega \text{ cm}^2$ ,  $133630 \Omega \text{ cm}^2$  and  $201700 \Omega \text{ cm}^2$ , while the double layer capacitance ( $Q_{dl}$ ) value was found to be  $16.57 \mu\text{F cm}^{-2}$ ,  $13.91 \mu\text{F cm}^{-2}$ ,  $11.51 \mu\text{F cm}^{-2}$ , and  $10.58 \mu\text{F cm}^{-2}$ , respectively. n values were 0.918, 0.933, 0.933 and 0.942, respectively. Compared to the Sn-Ni deposit, the charge transfer resistance ( $R_{ct}$ ) and n values increase when FG exists in Sn-Ni alloys, while the double layer capacitance ( $Q_{dl}$ ) decreases in Sn-Ni/FG1, Sn-Ni/FG2, and Sn-Ni/FG3. A decrease in  $R_{ct}$  and n values and an increase in  $Q_{dl}$  both occur in Sn-Ni/FG4. The increased  $R_{ct}$  values indicate that the addition of FG to the Sn-Ni coatings enhances the corrosion resistance of the coatings toward an aggressive environment. The decreased  $Q_{dl}$  and the increased n for Sn-Ni/FG composite coatings reveal the improved smooth microstructure and compactness of the coatings because of crystal refinement. The largest  $R_{ct}$  and the smallest  $Q_{dl}$  for Sn-Ni/FG3 deposited in the plating bath containing

300 mg L<sup>-1</sup> FG indicate the best corrosion resistance, and the well-fine crystal and compact layer for Sn-Ni/FG3 correspond to its excellent anti-corrosion performance. The deterioration of anti-corrosion for Sn-Ni/FG4 may be caused by the aggregation of FG in the plating bath because of its limited dispersibility. In fact, some nodular coatings can be observed in the bath with a high concentration of FG because large FG particles are embedded in the coatings. Hence, a suitable amount of well-dispersed FG is very important for an Sn-Ni/FG composite coating with good corrosion resistance to an aggressive environment.

To determine the degree of dissolution of the individual components and the anti-corrosion ability of metal or metallic alloys in a medium, the anodic polarization technique can be employed. Anodic polarization curves of the Sn-Ni deposits and Sn-Ni/FG3 composite coatings on the copper electrode were obtained in 5% NaCl solution at 10 mV s<sup>-1</sup> and are shown in Fig. 8. For Sn-Ni coatings, there are two anodic peaks, corresponding to the anodic reaction of metallic species in the Sn-Ni alloy, in which the anodic peak at 0.03 V is related to the dissolution of Sn in the alloy and the peak appearing at 0.25 V-3.0 V corresponds to the dissolution of Ni [10]. When the anodic polarization voltage extends to a more positive value, Sn-Ni alloy passivation takes place because of nickel passivation. No evident Sn dissolution appears in the Sn-Ni/FG composite coatings. Similar passivation behavior for Sn-Ni/FG3 composite coatings occurs except for it exhibiting a lower blunt current density. The blunt current density for Sn-Ni/FG3 is much lower than that of Sn-Ni alloys, indicating that the addition of FG to Sn-Ni improves the corrosion resistance of Sn-Ni alloys. The effect of FG on the corrosion resistance of Sn-Ni can be explained by the electrochemical reaction process occurring at the electrode/electrolyte interface. Under anodic polarization conditions, Sn and Ni that are exposed to the electrolyte will be oxidized to form oxides or hydroxides that will cover the electrode surface. For Sn-Ni/FG composite coatings, no evident Sn dissolution and a strong coating passivation indicate that Sn-Ni/FG coatings exhibit better self-passivation ability in air. Meanwhile, FG is impermeable, and the FG in the Sn-Ni matrix will inhibit ion transport, which decreases the attack on the Sn-Ni alloy by the electrolyte. In addition, a higher polarization resistance ( $R_p$ ) value also increases the difficulty of electrochemical reactions. Therefore, a lower anodic current density will be produced for the Sn-Ni/FG composite electrode, which contributes to better corrosion resistance in NaCl solution.

#### 4. CONCLUSION

Sn-Ni/FG composite coatings were successfully electrodeposited on copper substrates by dispersing functionalized fluorographene in a Sn-Ni alloy plating bath. The addition of FG changes the morphology of Sn-Ni from semispherical to an interlock ridge shape. With the increase in the FG content of the coatings in a reasonable range, the grain size of the composite tends to decrease. Compared to the pure Sn-Ni alloy coatings, a significant increase in the polarization resistance and decrease in the corrosion rate were observed for the Sn-Ni/FG composite coatings. In this work, the corrosion resistance rate increased with an increase in the amount of FG in the coatings when the content of FG in the bath was below 300 mg L<sup>-1</sup>, while the microstructure of the layer became more compact. The corrosion rate increased again when an excess amount of FG existed in the plating bath because of the limited

dispersion stability. A smaller grain size, compact layer, and hindered ion diffusion were responsible for the good corrosion resistance of Sn-Ni/FG composite coatings to an aggressive environment.

## References

1. S.K. Jalota, *Met. Finish.* 99(2001) 320.
2. S.A.M Refaey, F. Taha and T.H.A. Hasanin, *Electrochim. Acta.* 51(2006) 2942.
3. H. Jimenez, L. Gil, M.H. Staia and E.S. Puchi-Cabrera, *Surf. Coatings Technol.*, 202(2008): 2072
4. B. Subramanian, S. Mohan and S. Jayakrishnan, *J. Appl. Electrochem.*, 37(2007) 219.
5. T. Kobayashi, T.K.H. Kanematsu, M. Yoshitake and T. Oke. *Trans. IMF*, 80(2002) 194.
6. R. Sekar, C. Eagammai and S. Jayakrishnan, *J. Appl. Electrochem.*, 40(2010) 49.
7. W.X. Zhang, Z.H. Jiang, G.Y. Li, Q. Jiang and J.S. Lian, *Surf. Coatings. Technol.*, 202 (2008): 2570
8. Y. Zou, Y.H. Cheng, L. Cheng and W. Liu, *Mater. Trans.*, 51 (2010) 277
9. 9.C.Y. Wan, L. Zhang and X.Y. Liu, *Int. J. Electrochem. Sci.*, 15(2020) 26
10. 10.C.Y. Wan, X.Y. Liu and J.Y. Ye. *Surf. Coatings Technol.* 369 (2019) 244
11. 11. E.W. Brooman, *Met. Finish* 99(2001) 100
12. 12.A.C. Hegde, S. Shetty, M.M. J. Sadiq and D. K. Bhat, *RSC Adv.*, 6(2016) 77465
13. 13. B. Kucharska, A. Brojanowska, K. Poplawski and J.R. Sobiecki., *Mater. Sci. Medziagotyra.* 22(2016) 31.
14. 14. P. Ledwig and B. Dubiel. *Archives Metallurgy Mater.* 62(2017) 2455
15. 15. J.A. Caderon, J.E. Henao and M.A. Gomez. *Electrochim. Acta*, 124(2014) 190
16. 16. H. Karabulut, K. Karacif, R. Citak and H. Cinici. *Mater. Testing.* 63(2021) 1157
17. 17. J.H. Liu, Z.L. Pei, W.B. Shi, Y.D. Liu, J. Gong and C. Sun, *Surf. Coatings Technol.* 385(2020) 125451
18. 18. S. Arora, N. Kumari and C. Srivastava. *J. Alloys Compounds.* 801(2019) 449.
19. 19.M. Balasubramaniam and S. Balakumar, *Mater. Lett.*, 182(2016) 63.
20. 20. C.M. Seah, B. Vigolo, S.P. Chai and A.R. Mohamed, *Carbon*, 105(2016) 496.
21. 21. L.L. Zhao, X.Y. Liu, C.Y. Wan, X.R. Ye and F.H. Wu. *J. Mater. Eng. Perf.* 27 (2018) 875.
22. 22. D. Kuang, L.Y. Xu, L. Liu, W.B. Hu and Y.T. Wu, *Appl. Surf. Sci.* 273(2013) 484
23. 23. M.Y. Rekha, A. Kamboj and C. Srivastava, *Thin Solid Films*, 653(2018) 82
24. 24. C.M. Praveen Kumar, T.V. Venkatesha and R. Shabadi, *Mater. Res. Bulletin*, 48 (2013) 1477.
25. 25. R.Y Zhang, X. Yu, Q.W. Yang, G. Cui and Z.L. Li, *Constr. Building Mater.*, 294(2021) 123613
26. 26. A. Siokou, F. Ravani, S. Karakalos, O. Frank, M. Kalbac and C. Galiotis, *Appl. Surf. Sci.*, 257(2012) 9785
27. 27. H. Algul, M. Tokur, S. Ozcan, M. Uysal, T. Cetinkaya, H. Akbulut and A. Alp, *Appl. Surf. Sci.* 359(2015) 340.
28. 28. R.R. Nair, W.C. Ren, R. Jalil, I. Riaz, V.G. Kravets, L. Britnell, P. Blake, F. Schedin, A.S. Mayorov, S.J. Yuan, M.I. Katsnelson, H.M.Cheng, W. Strupinske, L.G. Bulusheva, A.V. Okotrub, I.V. Grigorieva, A.N. Grigorenko, K.S. Novoselov and A.K. Geim, *Small*, 6(2010) 2877.
29. 29. D. C. Elias, R.R. Nair, T.M.G. Mohiuddin, S.V. Morozov, P. Blake, M.P. Halsall, A.C. Ferrari, D.W. Boukhvalov, M.I. Katsnelson, A.K. Geim and K.S. Novoselov, *Science*, 323(2009) 610
30. 30. J.Y. Du, J.F. Liu, P.W. Gong, M. Tian, L. Sun, S.J. Ji, L. Zhang and Z. Liu, *Mater. Lett.* 196(2017) 165.
31. 31. C.B. Sun, Y.Y. Feng, Y. Li, C.Q. Qin, Q.Q. Zhang and W. Feng, *Nanoscale*, 6(2014) 2634.
32. 32.K.J. Jeon, Z. Lee, E. Pollak, L. Moreschini, A. Bostwick, C.M. Park, R. Mendelsberg, V. Radmilovic, R. Kostecke, T.J. Richardson and E. Rotenberg, *ACS Nano.* 5(2011) 1042.
33. 33. R. Romero-Aburto, T.N. Narayanan, Y. Nagaoka, T. Hasumura, T.M. Mitcham, T. Fukuda, P.J. Cox, R.R. Bouchard, T.Maekawa, D.S. Kumar, S.V. Torti, S.A. Mani and P.M. Ajayan, *Adv. Mater.*,

25(2013) 5632

34. 34. Y. Yang, G.L. Lu, Y.J. Li, Z.Z. Liu and X.Y. Huang, *ACS Appl. Mater. Interfaces*, 5(2013) 13478

35. 35.M. Pulikkathara, O. Kuznetsov and V.N. Khabashesku, *Chem. Mater.*, 20(2008) 2685

36. 36. C.Y. Wan and M. Ma, *J. Poros Mater.* 27(2020) 1319

37. 37. L. Shi, C.F Sun and W.M. Liu, *Appl. Surf. Sci.*, 254 (2008) 6880

38. 38. C. Schmetterer, H. Flandorfer, K.W. Richter, U. Saeed, M. Kauffman, P. Roussel and H. Ipser, *Intermetallics*, 15(2007) 869

39. 39. A.J. Cooper, N.R. Wilson, I.A. Kinloch and R.A.W. Dryfe, *Carbon*, 66(2014) 340.

© 2022 The Authors. Published by ESG ([www.electrochemsci.org](http://www.electrochemsci.org)). This article is an open access article distributed under the terms and conditions of the Creative Commons Attribution license (<http://creativecommons.org/licenses/by/4.0/>).